Applied Catalysis B: Environmental 165 (2015) 316–327

Contents lists available at ScienceDirect

Applied Catalysis B: Environmental

journal homepage: www.elsevier.com/locate/apcatb

Hybrid catalysts—an innovative route to improve catalyst performance in the selective catalytic reduction of NO by NH_3

Mariam Salazar, Ralf Becker[1], Wolfgang Grünert*

Lehrstuhl für Technische Chemie, Ruhr-Universität Bochum, D-44780 Bochum, Germany

ARTICLE INFO

Article history:
Received 7 July 2014
Received in revised form 6 October 2014
Accepted 7 October 2014
Available online 14 October 2014

Keywords:
Selective catalytic reduction
NH_3-SCR
$DeNO_x$
NO oxidation
Fe-ZSM-5
Manganese oxide
Hybrid catalyst.

ABSTRACT

The selective catalytic reduction (SCR) of NO by NH_3 was investigated over mechanical mixtures consisting of an oxidation catalyst and Fe-ZSM-5 as a component active for SCR. Oxidation components used included several metal oxides MO_x, where M is Mn, Mn–Ce, Mn–Cr, Mn–Cu, Ce–Zr, Mn/Ce–Zr. By comparing SCR rates and selectivities obtained with these mixtures ("hybrid catalysts") with those of their individual components, significant, sometimes drastic synergistic effects between both components could be established. Mn-based oxidation components, which provide high SCR activity on their own, were improved with respect to selectivity towards N_2 by the presence of Fe-ZSM-5. A strong synergy with clearly improved N_2 selectivity remained after the SCR activity of the Mn-containing phases was suppressed by thermal ageing. With the Ce–Zr oxidation component, lower activities were achieved, however at very high selectivity. The measurement of NO oxidation rates could not prove the basic idea of the oxidation catalyst providing NO_2 and enabling Fe-ZSM-5 to react the remaining NO via a fast SCR path. While the trends concerning synergy and NO oxidation activity were generally parallel, the NO oxidation activity of Fe-ZSM-5 in the absence of NH_3 exceeded or equaled that of most oxidation components which provided significant synergetic effects. For proving the mechanism, data on NO_2 formation in the presence of NH_3 are needed, which can be made available only by kinetic modeling as the $NO/NH_3/O_2$ system prefers the SCR route over NO oxidation. With Cu- and Cr-containing systems, unexpected changes in selectivity (N_2O formation) were noted upon thermal stress, the reasons of which remain unclear.

1. Introduction

Producers and researchers of catalysts for NO_x abatement are facing considerable challenges due to more stringent regulations regarding NO_x emissions. This creates the need for ever new catalysts for the selective catalytic reduction (SCR) of nitrogen oxides that provide high activity, selectivity, stability, and poisoning resistance in a broad range of operating temperatures. In particular, an attractive performance already at the relatively low temperatures of a diesel exhaust has become a critical issue because the current commercial catalysts based on V_2O_5–WO_3/TiO_2 cannot completely remove NO_x below 523 K [1]. Many studies have been devoted to the development of traditional metal oxide supported catalysts for low-temperature SCR applications, e.g. Cu zeolites, unsupported, and supported Mn oxides [1–9]. Recently, Stakheev et al. [10] have introduced catalyst combinations as a non-conventional principle which might result in catalysts providing excellent catalytic properties.

The basic idea is based on the fact that the SCR of NO/NO_2 mixtures (Eq. (1)) is much faster than the SCR of NO alone (Eq. (2)).

$$NO + NO_2 + 2NH_3 \rightarrow 2N_2 + 3H_2O \quad (1)$$

"fast SCR"

$$4NO + 4NH_3 + O_2 \rightarrow 4N_2 + 6H_2O \quad (2)$$

"standard SCR"

In $DeNO_x$ technology, a catalyst for NO oxidation (Eq. (3)) is therefore located upstream the SCR catalyst.

$$NO + {}^1/_2O_2 \rightarrow NO_2 \quad (3)$$

The reducing agent (NH_3 or urea) has to be fed downstream the oxidation catalyst to prevent its conversion over the latter [11]. The SCR catalyst operates according to Eq. (1) which allows for high conversions at low temperatures.

* Corresponding author at: Lehrstuhl für Technische Chemie, Ruhr-Universität Bochum, P.O. Box 102148, D-44780 Bochum, Germany. Tel.: +49 234 322 2088; fax: +49 234 321 4115.
E-mail address: w.gruenert@techem.rub.de (W. Grünert).
[1] Sachtleben Pigment GmbH, 47829 Krefeld, Germany.

http://dx.doi.org/10.1016/j.apcatb.2014.10.018
0926-3373/

Stakheev et al. have shown that it is possible to combine an oxidation catalyst and an SCR catalyst in the form of a mechanical mixture to promote SCR reaction in typical exhaust gases where the nitrogen oxides consist mainly of NO (>90%) [10]. For this combination to be successful, the oxidation catalyst has to be highly active for NO oxidation, but not to the same extent for ammonia oxidation. Using Fe-Beta as an SCR catalyst, Stakheev et al. showed that Ce–Zr mixed oxides, in particular, if doped with Mn species, apparently serve this purpose and allow for attractive activity of the mechanical mixtures.

We report here results of a further exploration of this principle of hybrid SCR catalyst systems. Using Fe-ZSM-5 as the SCR component, we selected a series of metal oxides as the oxidation component: Mn oxides, composite Mn oxides and, for comparison, cerium–zirconia mixed oxide. Mn oxide-based catalysts are known to catalyze NH_3-SCR at very low temperatures [1–3], but with poor selectivity for N_2 due to their high activity towards oxidation reactions. This oxidation capability could be beneficial in combined (hybrid) catalysts. On the other hand, the tendency of Mn to N_2O formation might permit a differentiation between contributions of the catalyst components because Fe-ZSM-5 forms nitrogen with very high selectivity in standard, as well as in fast SCR [12,13]. Unsupported Mn oxides are known to be very unstable, therefore mixed oxide systems the stability of which is improved by a second component such as Ce or Cr [5,14] are also included. The oxidizing potential of Ce–Zr–O mixed oxide, which arises from its tendency to form oxygen vacancies down into subsurface regions, is well known [15,16]. The Fe content of the Fe-ZSM-5 SCR component was chosen to be small in order to obtain a catalyst with only modest activity in standard SCR but at the same time high activity in fast SCR [13]. This allows for sufficient space to observe synergetic effects that might be caused by the formation of NO_2 and a resulting shift of the reaction system from Eq. (2) to Eq. (1).

2. Experimental

2.1. Catalyst preparation

Fe-ZSM-5 was prepared by solid-state ion exchange (SSIE) following a procedure described in detail by Schwidder et al. [13]. In brief, a commercial NH_4-ZSM-5 (Si/Al ≈ 14) provided by Tricat Zeolites, Bitterfeld, now a Clariant company, was transferred into the H form by calcination in synthetic air (20.5% O_2 in N_2 or He) at 773 K for 5 h. This H-ZSM-5 was ground vigorously with a given amount of $FeCl_3{\cdot}6H_2O$ and heated at 573 K for 1 h in inert gas. Then, the sample was washed with deionized water to remove chlorides and dried at ambient atmosphere. Finally, the sample was calcined in synthetic air at 873 K for 2 h.

Several manganese oxides were combined with this Fe-ZSM-5, including pure MnO_x, MnO_x–CeO_y, MnO_x–CrO_y, and MnO_x–CuO_y. Manganese mixed oxides have been reported to provide interesting catalytic properties in NH_3-SCR [1,4–9]. Pure manganese oxides were generated by precipitation (P) and by the citric-acid route (CA) while Mn–Ce–O and Mn–Cr–O mixed oxides materials were made via the CA route only. The corresponding samples will be labeled Mn(P), Mn(CA), and Mn-X(CA), with X representing Ce or Cr. MnO_x–CuO_x mixed oxides are sometimes referred to as hopcalites. The samples used in our work were supplied by Cardiff University (Mn–Cu(1)) and by Carus Corporation (Mn–Cu(2)). Mn–Cu(1) was prepared according to procedures described in [17], while Mn–Cu(2) is on the market under the product name Carulite 300.

The precipitation method consisted in adding aqueous sodium carbonate (0.5 M) to manganese nitrate solution (0.5 M) up to a pH of 8. The resulting precipitate was aged at room temperature for 1 h, filtered, washed several times with hot distilled water, dried and calcined at 623 K for 3 h. In the citric acid route, manganese nitrate or mixtures of it with Cr or Ce nitrate were used, with a molar ratio X/(X + Mn) of 0.5 (X = Cr or Ce). The molar ratio of citric acid to the metal components (sum of X and Mn) was set to 1 and the molarity (X + Mn) to 0.5 M. The resulting solutions were stirred at room temperature for 1 h. Later, the solution was dried at 423 K for around 12 h, which resulted in a porous, foam-like solid. This precursor was calcined at a final temperature of 923 K for 3 h in synthetic air using a rotary furnace.

Ceria-zirconia mixed oxide was supplied by Umicore AG & Co. KG. This material was also loaded with 5 wt% MnO_2 by impregnation with an aqueous solution of $Mn(NO_3)_2$ followed by drying and calcination in synthetic air at 823 K for 1 h. These samples will be labeled Ce–Zr and Mn/Ce–Zr.

For preparing the hybrid catalysts, these oxidation components were mixed with Fe-ZSM-5 at a weight ratio 1/1. The corresponding mixture was thoroughly ground in a mortar, pressed, crushed, and sieved to obtain an appropriate particle size for the catalytic evaluation (250–350 μm, 45–60 mesh). The hybrid catalysts have been labeled as Y + FeZSM5, where Y refers to the oxidation component.

2.2. Catalyst characterization

Textural characterization was obtained from nitrogen adsorption–desorption isotherms measured at 77 K with a NOVA-2000 instrument (Quantachrome). The samples were outgassed at 573 K under a residual pressure of 10^{-3} mbar for 3 h. Surface areas were evaluated from the BET model.

The phase compositions of the fresh catalyst components and of some catalysts treated under similar conditions as in the SCR reaction (calcination at 873 K/1 h) were characterized by X-ray powder diffraction measurements. Patterns were recorded in reflection geometry with an Empyrean Theta-Theta diffractometer (Panalytical, Almelo) equipped with a Cu anode (λ = 1.54056 Å), 0.25° divergent slit, 0.5° antiscatter slit (incident beam), 7.5 mm high antiscatter slit (diffracted beam), incident and diffracted beam 0.04 rad soller slits, and a position-sensitive PIXcel-1d detector. The K-beta emission line was suppressed by a Ni Filter. The specimens were scanned in the 5–80° 2θ range (step width, 0.0131°; collection time, 250 s) at ambient temperature. The crystalline phases were identified by comparison with reference data from International Center for Diffraction Data (ICDD) files. Particle sizes of mixed metal oxides were calculated by using the Scherrer equation, which was applied to the (311), (511), and (440) reflections of the observed spinel phases.

Photoemission measurements (XPS, X-ray induced Auger spectroscopy) have been made to examine a special feature with Cu-containing catalysts. They were performed on two different instruments for technical reasons, one of them (Bochum) equipped with a monochromatized Al Kα source and a Gammadata-Scienta SES 2002 analyzer, the other one (at Fritz Haber Institute of Max-Planck Society in Berlin) equipped with twin-anode and a Phiobus analyzer from Specs. The energy scale of the spectra was referenced to the line of adventitious carbon (C 1s binding energy of 284.5 eV).

Elemental analysis was made by ICP-OES, using a UNICAM PU 701 spectrometer. The dissolution of the samples was accomplished using nitrohydrochloric acid (Cu–Mn mixed oxides) or peroxide fusion (Cr–Mn and Ce–Mn mixed oxides).

2.3. Catalytic measurements

Catalytic data were measured for three reactions: for the target reaction standard SCR, for NO oxidation, and in the case of Fe-ZSM-5 also for fast SCR. The reactions were carried out in flow regime using a microflow quartz reactor (4.2 mm i.d.) inserted into an electric tubular furnace. Gas lines after and before the reactors were

heated to avoid condensation of water and ammonium nitrate formation. The reactions were carried out at atmospheric pressure at temperatures between 373 and 873 K.

During the catalytic measurements, the GHSV was adjusted to 300,000 h^{-1} for the hybrid catalysts and to 600,000 h^{-1} for the individual components in order to identify the contribution of each component to activity and selectivity in the final hybrid system. For this purpose, 25 mg (hybrid catalysts) or 12.5 mg (individual components) were loaded into the reactor. For standard SCR, the feed consisted of 1000 ppm NO, 1000 ppm NH_3, 2 vol% O_2, balanced with He. After completion of the first run at 873 K, the reactor was cooled down to room temperature, and a second identical run was carried out. This second run was meant to provide initial insights into the changes caused by exposure to high temperatures. Such changes were expected in cases where oxidation components calcined at low temperatures had been used, but they may generally arise from interactions between oxidation component and zeolite, or due to special effects of the reactant present at high temperatures (as opposed to air present during calcination).

For NO oxidation, the same feed was used as mentioned above, but with NH_3 replaced by He. This reaction was carried out with the individual components and with some of them after having been exposed to SCR conditions at 673 K for 30 min. Both fresh catalysts and those exposed to SCR feed were evaluated at 300,000 h^{-1}. For fast SCR over Fe-ZSM-5, the standard SCR feed was changed by a replacing 1000 ppm NO by a mixture of 500 ppm NO and 500 ppm NO_2, the GHSV was 600,000 h^{-1}.

In the steady state, NO, NO_2, and NH_3 concentrations were analyzed on-line using an XStream X2 Gas Analyzer (Rosemount Analytical; Emerson) which combines non-dispersive infrared and ultraviolet spectrometry for quantitative determination. Additionally, N_2O was quantified using a quadrupole mass spectrometer (Omnistar, Pfeiffer) calibrated by the internal standard method while N_2 yield in Fig. 6 was evaluated from the balance.

Conversions were calculated according to the following equations (i-NO or NH_3):

$$X_i\,(\%) = \frac{c_{i,in} - c_{i,out}}{c_{i,in}} \times 100\%$$

The byproduct formation is reported by the concentrations of N_2O and NO_2 obtained.

3. Results

3.1. Characterization

In Table 1, the textural properties and chemical composition of individual catalysts are summarized. The BET surface areas of Mn phases used in composite materials span a wide range from 242 to 21 m^2/g. This could be a result of different temperatures during final calcination: solids calcined at 923 K (Mn(CA), Mn–Cr(CA), and Mn–Ce(CA)) exhibit lower surface areas than Mn(P), which was calcined at 623 K (21–35 m^2/g vs. 127 m^2/g). Consequently, the high surface areas of Mn–Cu materials (123–242 m^2/g) suggest that their preparations included thermal treatment only at low temperature. From Table 1, it can also be seen that the Mn–Ce and Mn–Cr mixed oxides contain a high amount of manganese in agreement with the intended 0.5 molar fraction (X/X + Mn) in the precursors. The compositions of both Mn–Ce and Mn–Cr oxides are close to the targeted ones. The Mn/Cu ratio of the two hopcalites differs slightly. The Fe content of Fe-ZSM-5 is 0.4 wt%.

In Fig. 1A, the XRD patterns of the fresh catalyst components are given. Several dominating phases can be discerned. Mn(P), for instance, exhibited broad diffraction peaks corresponding to $MnCO_3$, which indicates that the calcination temperature of 623 K was not sufficient to completely decompose the precipitated

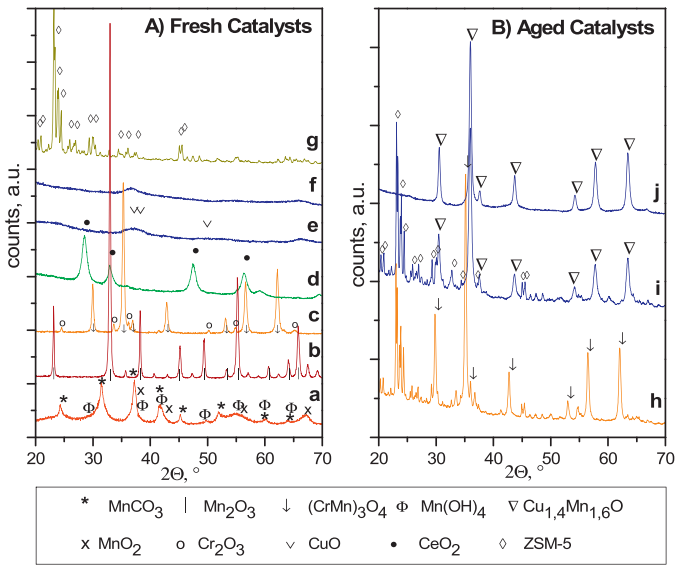

Fig. 1. XRD patterns of (A) individual catalyst components (left side): (a) Mn(P), (b) Mn(CA), (c) Mn-Cr, (d) Mn–Ce, (e) Mn–Cu(1), (f) Mn–Cu(2), (g) Fe-ZSM-5; and (B) aged catalysts (right side): (h) aged Mn–Cr + FeZSM5, (i) aged Mn–Cu(1) + FeZSM5, (j) aged Mn–Cu.

manganese carbonate. Weak diffraction peaks that might be assigned to MnO_2 and $Mn(OH)_4$ were also found. The low signal intensity indicates a highly disordered structure of this sample in agreement with the high surface area found for it, whereas intense and sharp lines of Mn_2O_3 were seen for high-temperature calcined Mn(CA). A minor component also present in this sample could not be identified.

The mixed oxides prepared via the CA route gave rather different diffractograms. While pure manganese compounds were not detected, the $(CrMn)_3O_4$ spinel caused intense signals in Mn–Cr(CA), but segregated Cr_2O_3 could be identified as well. In Mn–Ce(CA), only CeO_2 was detected from rather broad lines. The absence of crystalline MnO_x phases, which would readily form in the absence of Cr and Ce suggests, however, that there are amorphous mixed phases present in both cases because the suppression of Mn oxide crystallization most likely arises from the presence of Mn–O–X groups in the solids.

Very similar XRD patterns were found for the two Mn–Cu mixed oxides (hopcalites). They are completely amorphous. A very weak broad signal might arise from very small CuO crystallites. Finally, only diffraction peaks typical of zeolite ZSM-5 were identified for Fe-ZSM-5, no crystalline Fe phases could be detected.

The XRD patterns of the aged catalysts will be discussed further below.

3.2. DeNO$_x$ activity

To reveal the influence of the catalyst components in the catalyst mixture, NO and NH_3 conversions and concentrations of by-products are plotted in Figs. 2–5. Note that the space velocities are selected so that the data of the components show their expected contributions in the mixture if there was no synergistic effect. The diagrams b, e, and f report the data of the second run which were expected to give some preliminary information on stability.

Hybrid catalysts with pure manganese oxides show very high NO and NH_3 conversions at low and intermediate temperatures (Fig. 2), but lose their SCR selectivity above 700 K. Judging only from the conversions, the low-temperature performance of Mn(P) does not indicate a synergistic effect because the conversions of the oxide and its mixture with ZSM-5 are almost identical until

Table 1
Comparison of BET surface areas and chemical composition of individual catalysts.

	Calcination temperature (K)	BET surface area ($m^2\ g^{-1}$)	Mn (wt%)	Cr, Cu, or Fe (wt%)	Mn: (X +Mn) atomic ratio
Mn(P)	623	127	nd	–	–
Mn(CA)	923	21	nd	–	–
Mn–Ce(CA)	923	35	23	55	0.5
Mn–Cr(CA)	923	31	26	28	0.5
Mn–Cu(1)	Unknown	123	34	24	0.6
Mn–Cu(2)	Unknown	242	40	22	0.7
Fe-ZSM5	873	339	–	0.4	–

470 K (Fig. 2a). However, the well-known N_2O formation tendency of MnO_x catalysts [1–3] has been strongly decreased in the same temperature range (Fig. 2c). Fe-ZSM-5 is known to catalyze N_2O decomposition and selective reduction of N_2O by NH_3, but according to evidence available in literature [18,19] both reactions should be far too slow to explain this improvement in selectivity for N_2. At higher temperatures, a synergistic effect is visible also from the conversions, which are higher than the sum of conversions over the components up to 720 K. Mn(CA) alone is a poor catalyst, but it combines with Fe-ZSM-5 to make an attractive hybrid system, which is, however, somewhat less active than the mixture with Mn(P). At high temperatures (773–873 K), where Fe-ZSM-5 alone provides good conversions, the combinations are very unfavorable. Most likely, this is due to NH_3 being predominantly oxidized on Mn sites in this temperature range and therefore being unavailable for the fast SCR reaction over Fe-ZSM-5.

As expected, Mn(P) which was calcined at only 623 K suffered a breakdown by exposure to 873 K (Fig. 2b). The consequences for the hybrid catalyst were, however, rather moderate: its light-off temperature T_{50} (temperature of 50% conversion) shifted by just ca. 30 K, and the curve approached that of Mn(CA) + Fe-ZSM-5. While the conversion curve of the latter did not change significantly with exposure to the feed at 873 K, its tendency to release N_2O was further attenuated (Fig. 2a, b; c, e). In the conversion curves, the synergistic effect between the calcined Mn oxides and Fe-ZSM-5 is now obvious over the whole temperature range. However, although both the N_2O and the NO_2 selectivities are significantly reduced by the presence of Fe-ZSM-5, both oxides are still formed, which indicates a significant influence of the non-selective Mn in the complex reaction system.

Similar results were obtained when mixed manganese oxides with cerium and chromium oxides were employed as oxidation components (Fig. 3). In the conversion curves (Fig. 3a), the synergism between oxidation and SCR components can be observed from 573 K onwards. In the low-temperature range, the behavior of the hybrid catalysts resembles that of Mn(CA) + Fe-ZSM-5 (Fig. 2a), but at high temperatures, the NO conversions never become negative. Apparently, the mixed oxides are less active in the oxidation of ammonia, which is also reflected in a very low tendency to NO_2 formation in the 650–800 K temperature range where NH_3 conversion is complete (Fig. 3d and f). However, the hybrid catalysts with mixed oxides release more N_2O than Mn(CA) + Fe-ZSM-5 (Figs. 2c and 3c), and while N_2O formation is slightly attenuated after the first run over Mn–Ce(CA) + Fe-ZSM-5, it is strongly increased in the case of Mn–Cr(CA) + Fe-ZSM-5 (Fig. 3e). This surprising feature is reflected by an obvious change in the shape of the NO conversion curve of this mixture (Fig. 3b). The contrasting tendencies between NH_3 oxidation revealed at high temperatures and N_2O formation (Figs. 2 and 3) suggest that N_2O is formed from a reaction involving NO, e.g. via Eq. (5):

$$4NO + 4NH_3 + 3O_2 \rightarrow 4N_2O + 6H_2O \quad (5)$$

rather than from the reaction between NH_3 and O_2.

The spectacular results obtained with the hopcalites are presented in Fig. 4. While the hopcalites behaved similar when exposed to the feed alone, they differed drastically in combination with Fe-ZSM-5. The conversion curves of the pure hopcalites (Fig. 4a) resemble those of the Mn–Ce and Mn–Cr mixed oxides (Fig. 3a), but the even narrower ranges with positive NO conversion indicate a larger potential to catalyze NH_3 oxidation. This was dramatically suppressed by the exposure to 873 K (Fig. 4b): Both NO and NH_3 conversions remain almost zero up to 640 K. In combination with Fe-ZSM-5, Mn–Cu(1) + Fe-ZSM-5 was almost as active as Mn(P) + Fe-ZSM-5 (T_{50} = 441 and 433 K, respectively, cf. Figs. 2a and 4a), but with the Mn–Cu(1) hopcalite, NO conversions stayed positive over the whole temperature range. The hybrid catalyst with Mn–Cu(2) was somewhat less active (T_{50} = 573 K) and caused rather intense ammonia oxidation at high temperatures resulting in negative NO conversions (Fig. 4a). After exposure to 873 K (second run, Fig. 4b), the NO conversions of the mixtures remained remarkable although both NO and NH_3 conversions over the pure hopcalites were barely detectable up to 620 K. The light-off temperature of Mn–Cu(2) + Fe-ZSM-5 was increased by just 20 K while the loss in activity was more severe with the Mn–Cu(1) containing mixture (ΔT_{50} = 50 K). At higher temperatures, the conversion curves remained unchanged.

The behavior of the hopcalite-containing hybrids in the second run is rather surprising. The synergistic effect seems either to rely on just a few percent NO conversion to NO_2, which can hardly be detected with the pure components (Fig. 4f), or solid-state reactions between hopcalite and zeolite during the first run have resulted in major changes to the structure of the catalyst system. Unfortunately, the picture becomes less appealing when N_2O formation is included (Fig. 4c–f). It is already rather intense in the mixtures with the fresh hopcalites (Fig. 4c), and in this case, N_2O formation is even strongly increased by contact with the feed at 873 K (Fig. 4e).

The catalytic data for the ceria–zirconia-based catalysts are shown in Fig. 5. As reported in [10], a clear synergistic effect can be detected with Ce–Zr–O_x as well, but the activity is not comparable with that of the Mn-based systems: T_{50} is as high as 590 K (Fig. 5a). Addition of just 5 wt% MnO_2 brings it down to 510 K. This is at the expense of an unfavorable behavior at higher temperatures (Fig. 5a). In addition, the Mn component causes the formation of some N_2O and NO_2 though at moderate yields ($N_2O \leq 6\%$, $NO_2 \leq 5\%$ in fresh state, Fig. 5c and d). Exposure of these catalysts to 873 K did not cause significant changes (Fig. 5b, e, and f).

The results reported so far are summarized in Fig. 6 where N_2 and N_2O concentrations obtained at 523 K in the first and second runs are presented. From the graph, it can be seen that among the Mn-containing catalysts, Mn(CA) + FeZSM-5 gives the best N_2/N_2O ratio both in the fresh and used state, followed by Mn(P) + FeZSM-5. The latter provides the highest N_2 production in the used state. The high N_2O formation of the hybrids with Mn composite oxides is disappointing and tends to reject them from a practical perspective despite their attractive activities and stabilities. Regarding by-product formation, Ce–Zr + Fe-ZSM-5 is the cleanest choice, but also the least active. Impregnation with 5% MnO_2 improves activity strongly at moderate by-product formation. Our results with the pure Mn oxides suggest that a similar behavior may also be obtained without the ceria–zirconia component.

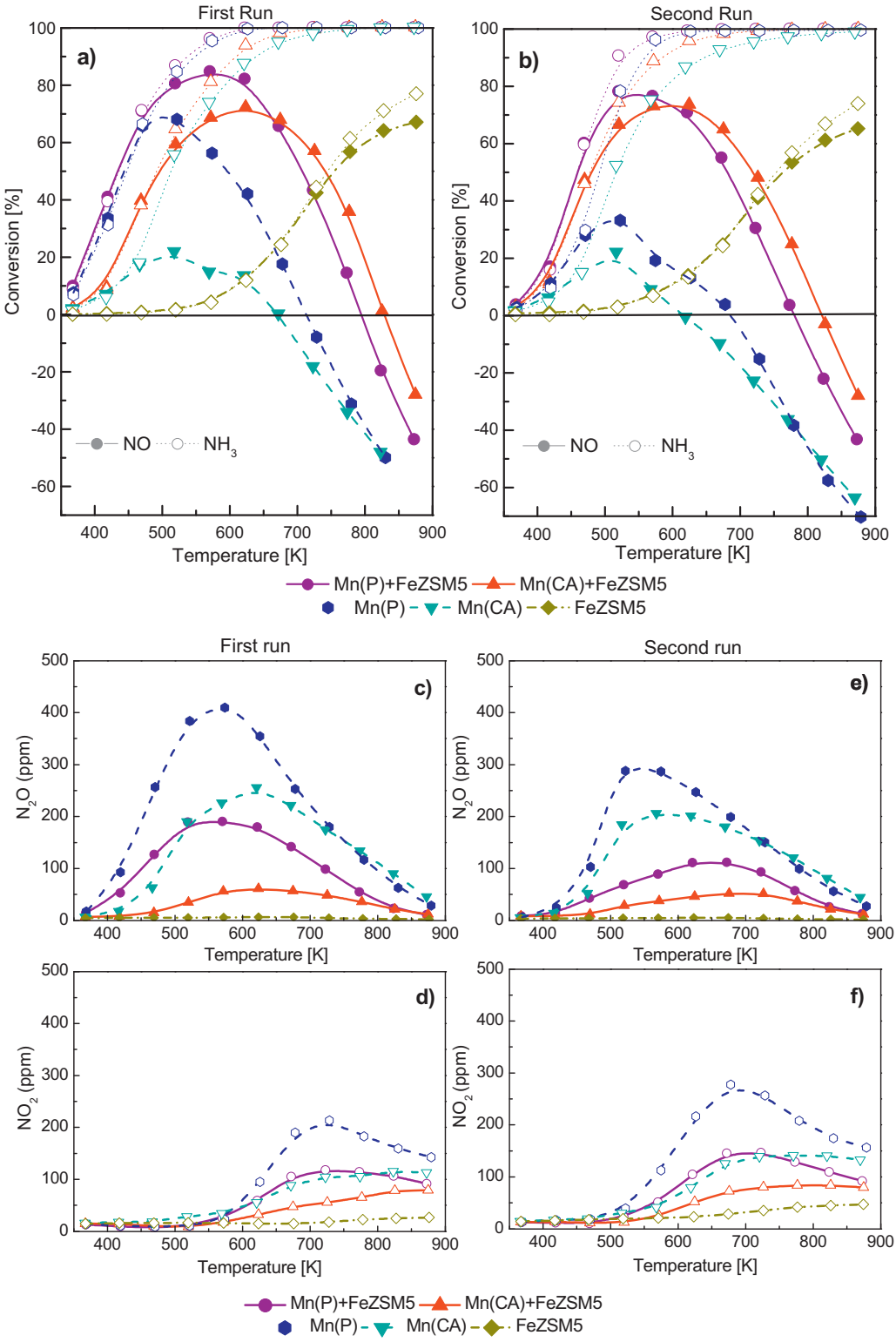

Fig. 2. NH_3-SCR measurements over individual and hybrid catalysts composed of pure manganese oxides and Fe-ZSM-5. (a, b) NO and NH_3 conversions: (a) fresh catalysts (first run), (b) aged catalysts (second run), (c–f) concentrations of by-products formed: (c, e) N_2O from fresh (c) and aged (e) catalyst, (d, f) NO_2 from fresh (d) and aged (f) catalyst. 1000 ppm NO, 1000 ppm NH_3, and 2% O_2 in He, GHSV = 300,000 and 600,000 h^{-1} for combined and individual catalysts, respectively.

3.3. *NO oxidation*

Based on the assumption that catalyst components promoting oxidation of NO to NO_2 enhance activity in SCR by enabling the fast SCR route, the NO oxidation activity of the individual components was studied. The NO conversion curves shown in Fig. 7 exhibit the well-known volcano shapes because NO conversion is limited by the NO/NO_2 equilibrium. All Mn-based samples are indeed very good catalysts for NO oxidation, with the notable exception of Mn–Cr(CA).

The highest NO conversions were obtained with Mn(P). Its activity for NO oxidation was only moderately affected by thermal stress

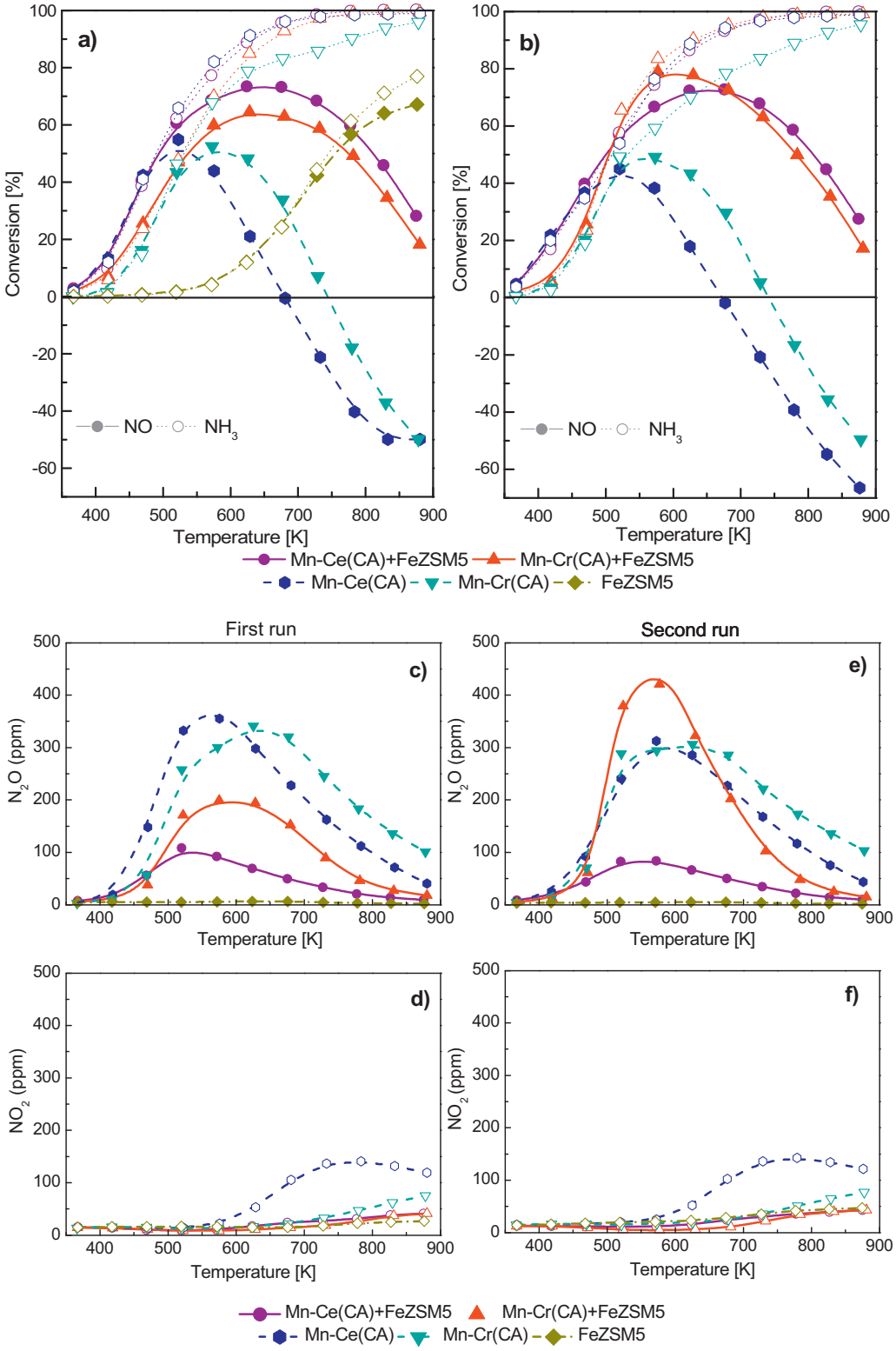

Fig. 3. NH_3-SCR measurements over individual and hybrid catalysts composed of mixed Mn–Ce or Mn–Cr oxides and Fe-ZSM-5. (a, b) NO and NH_3 conversions: (a) fresh catalysts (first run), (b) aged catalysts (second run), (c–f) concentrations of by-products formed: (c, e) N_2O from fresh (c) and aged (e) catalyst, (d, f) NO_2 from fresh (d) and aged (f) catalysts. For operation conditions, see Fig. 2.

(aged Mn(P) and Mn(CA), Fig. 7a). This is very different from the breakdown of its SCR activity (Fig. 2a and b), but is congruent with its synergistic effect with Fe-ZSM-5 and suggests that NO oxidation is crucial for the synergy observed. High NO oxidation activities were also observed with the hopcalites (Fig. 7b), however with Mn–Cu(2) being superior to Mn–Cu(1) unlike their influences in the hybrid catalysts (Fig. 4). In NO oxidation, Mn–Cu(1) is comparable to Mn–Ce(CA) and Mn-doped ceria–zirconia. As expected,

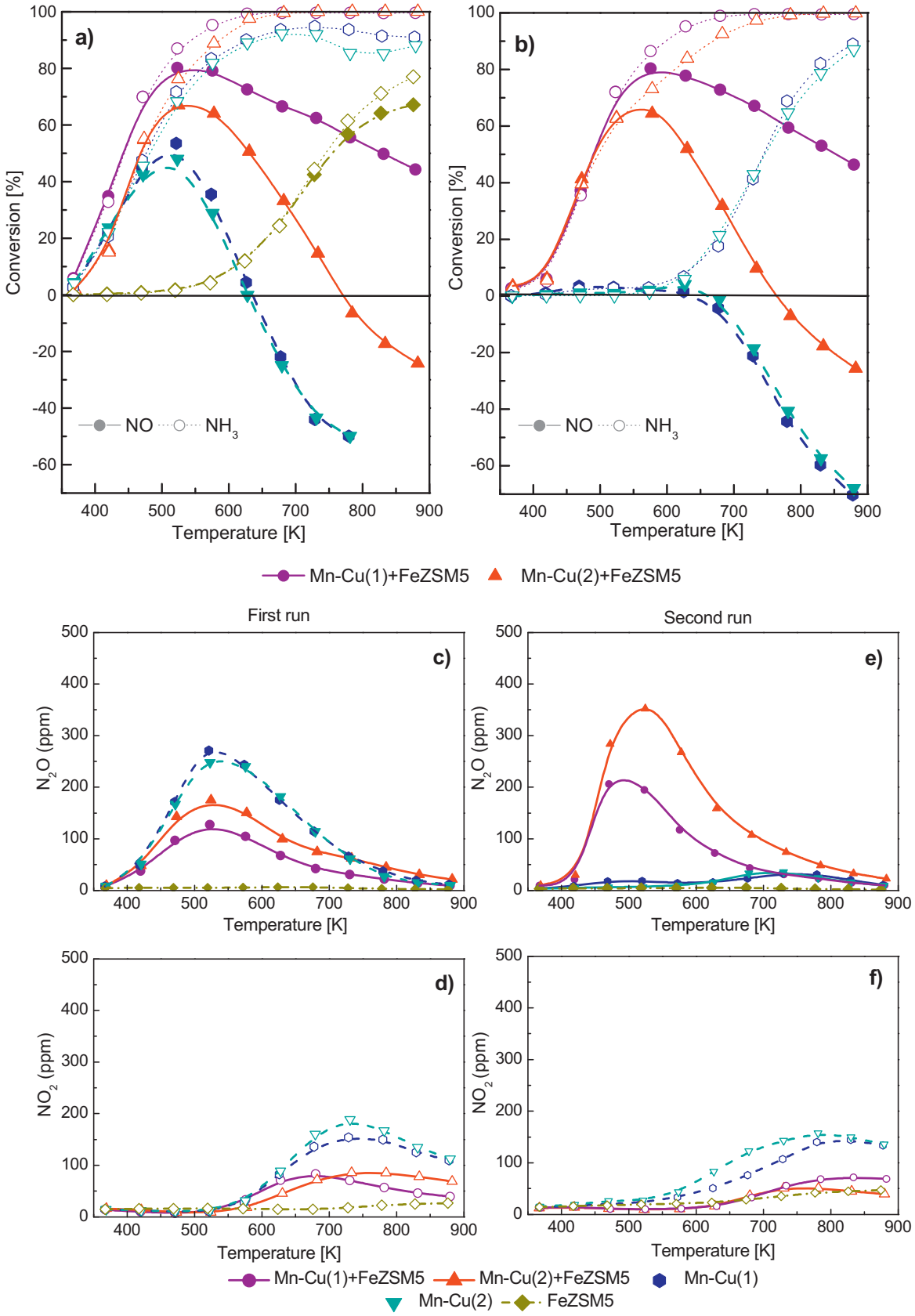

Fig. 4. NH_3-SCR measurements over individual and hybrid catalysts composed of mixed Mn–Cu oxides and Fe-ZSM-5. (a, b) NO and NH_3 conversions: (a) fresh catalysts (first run), (b) aged catalysts (second run), (c–f) concentrations of by-products formed: (c, e) N_2O from fresh (c) and aged (e) catalyst, (d, f) NO_2 from fresh (d) and aged (f) catalysts. For operation conditions, see Fig. 2.

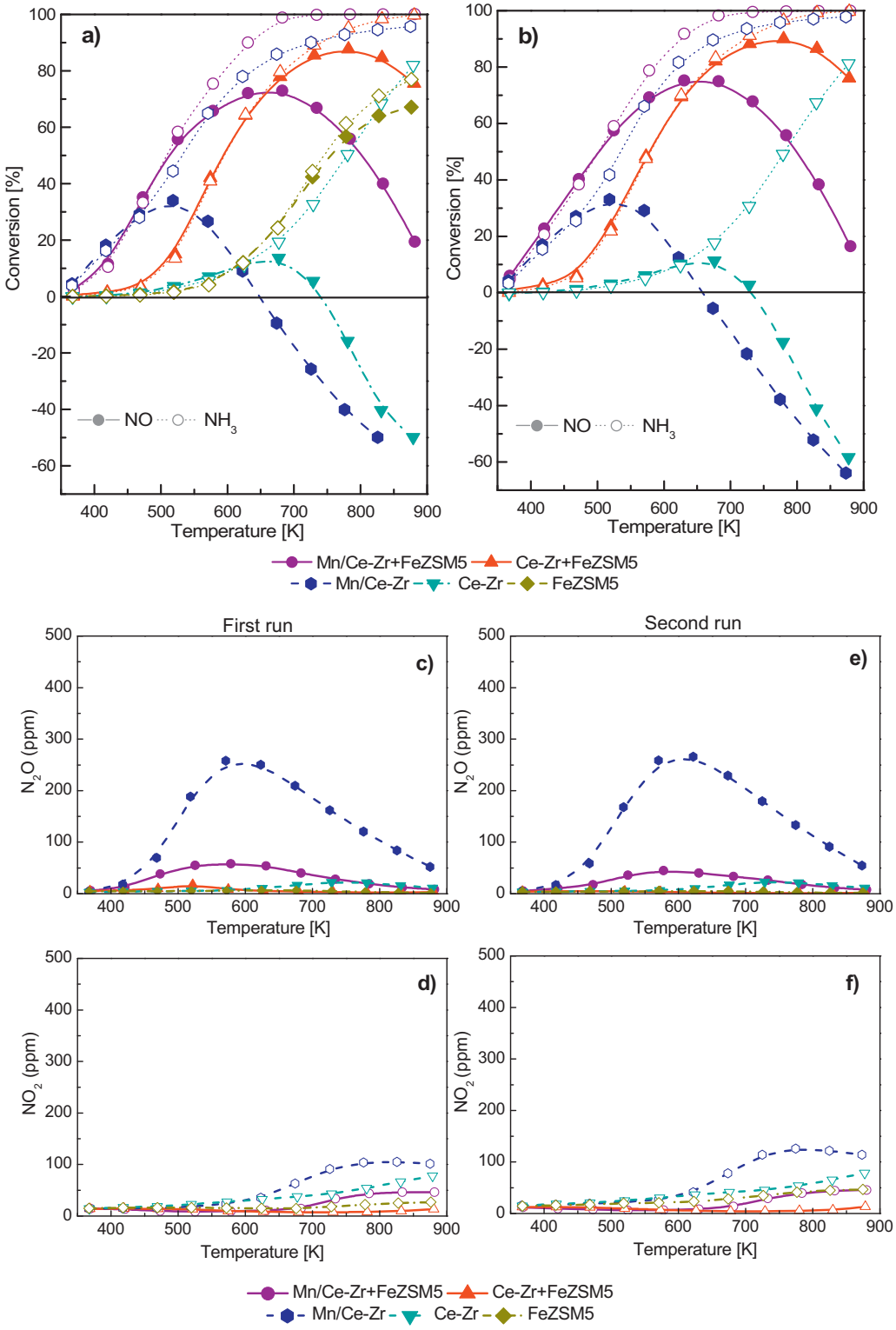

Fig. 5. NH_3-SCR measurements over individual and hybrid catalysts composed of Ce–Zr oxide or Mn/Ce–Zr oxide and Fe-ZSM-5. (a, b) NO and NH_3 conversions: (a) fresh catalysts (first run), (b) aged catalysts (second run), (c–f) concentrations of by-products formed: (c, e) N_2O from fresh (c) and aged (e) catalysts, (d, f) NO_2 from fresh (d) and aged (f) catalysts. For operation conditions, see Fig. 2.

Fe-ZSM-5 was among the poorest catalysts for NO oxidation when employed without any treatment (Fig. 7a). Notably, NO_2 formation rates over Mn–Cr(CA) did not significantly exceed those of Fe-ZSM-5 up to 520 K, and Ce–Zr–O_x provided less NO_2 than Fe-ZSM-5 even up to 670 K. However, both Mn–Cr(CA) and Ce–Zr reached equilibrium conversions at higher temperatures unlike the fresh Fe-ZSM-5 where conversions decreased while being still quite far from equilibrium.

Our group has recently found that the NO oxidation activity of Fe zeolites can be strongly boosted by a treatment which enforces redox cycling of the Fe sites, e.g. contact with SCR feed at temperatures above 623 K [20]. Therefore, NO oxidation was also carried

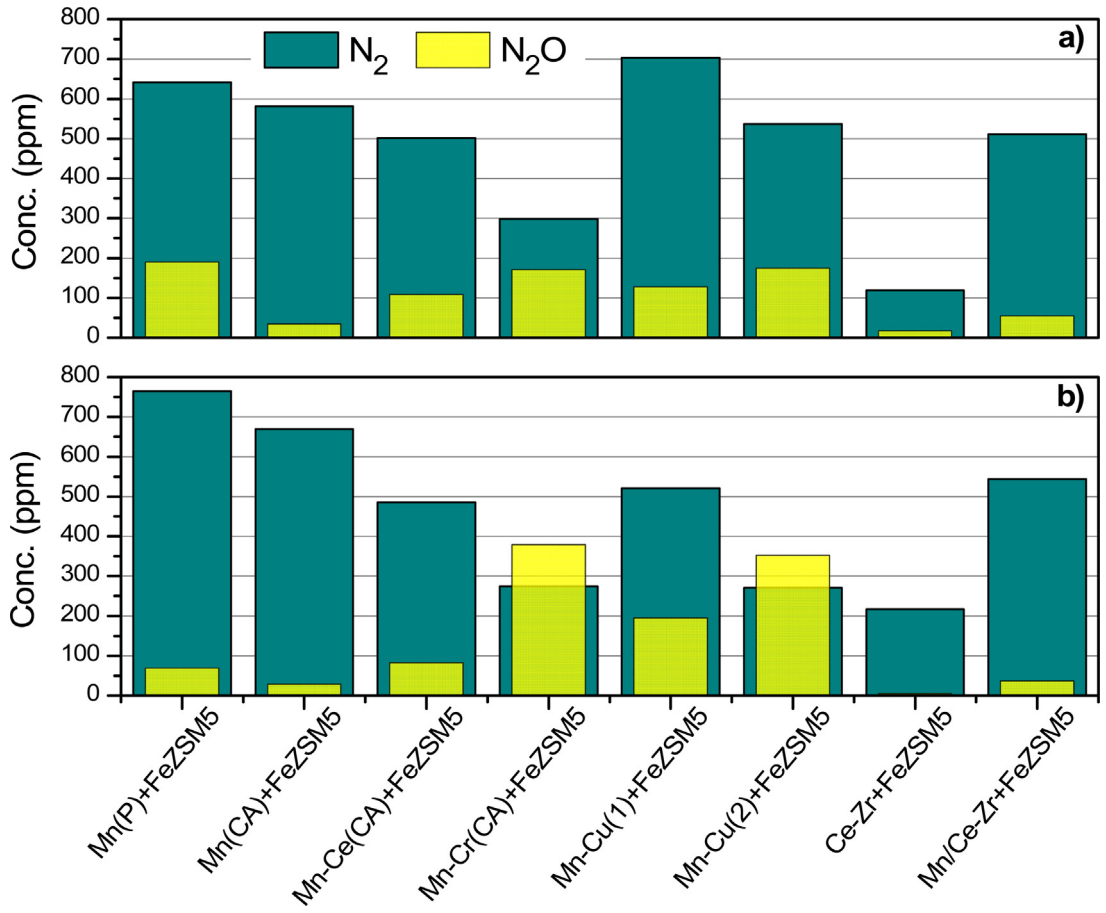

Fig. 6. Comparison of NH_3-SCR performance obtained with hybrid catalysts at 523 K. (a) fresh catalysts (first run), (b) aged catalysts (second run) (see Fig. 2 for operation conditions).

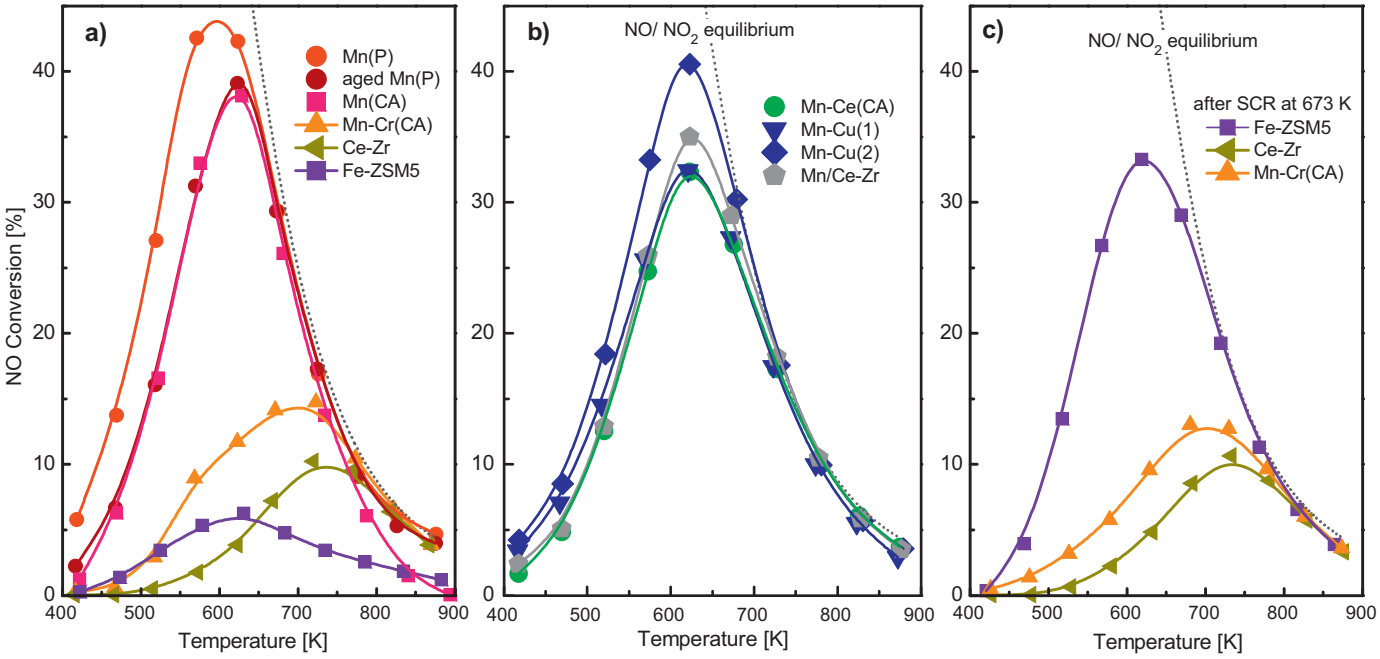

Fig. 7. NO oxidation over individual catalysts. (a, b) fresh catalysts, (c) after use in selective catalytic reduction (feed–s. Fig. 2) at 673 K. 1000 ppm NO and 2% O_2 in He, GHSV = 300,000 h^{-1}.

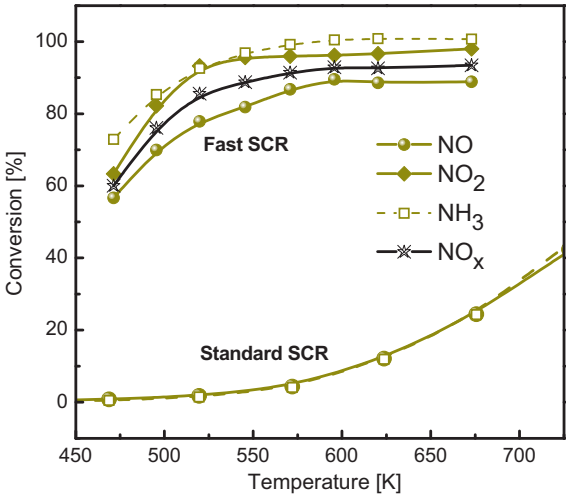

Fig. 8. Fast SCR reaction over Fe-ZSM-5. 500 ppm NO, 500 ppm NO_2, 1000 ppm NH_3, and 2% O_2 in He, GHSV = 600,000 h^{-1}. Conversion curves for standard SCR at the same GHSV are added for comparison.

out after contact with SCR feed at 673 K. Indeed, NO conversions achieved in this state (Fig. 7c) where much higher. The NO oxidation activity of Fe-ZSM-5 is now well comparable with that of some Mn-containing catalysts, e.g. Mn–Cu, Mn–Ce (Fig. 7a) and clearly above those of Mn–Cr(CA) and Ce–Zr, which were not strongly influenced by previous contact with the SCR feed (Fig. 7c).

3.4. Fast SCR

The fast SCR reaction over Fe-ZSM-5 was studied to evaluate its potential contribution to the total SCR rate and the selectivity of the combined systems. As in standard SCR, evidence of by-product formation was not found in fast SCR, it was completely selective towards N_2. Fig. 8 shows that the conversions of all reactants reached a flat plateau above 573 K. Actually, NO_2 conversions always somewhat exceeded that of NO, and NH_3 conversion was larger than the average of NO and NO_2 conversions. For low temperatures, NH_4NO_3 formation from NH_3 and NO_2 might be considered as a reason for this, but the N_2O expected from the reaction was not detected, and the temperatures covered in Fig. 8 are mostly above the decomposition point of the nitrate. Therefore, we rather suggest that some NH_3 may become oxidized to N_2 by active surface oxygen arising from NO_2, which would be converted, e.g. to NO. This is supported by the larger NH_3 conversions. Therefore, NO_2 conversions reached the plateau at 50 K earlier than the other components. The maximum conversions varied according to the reactant, they were 89% for NO, 94% for NH_3, and 98% for NO_2. NO and NH_3 conversions from standard SCR are repeated in the figure for comparison. As expected, the reaction rates in presence of NO_2 are larger by orders of magnitude.

4. Discussion

The results reported above present ample evidence for synergistic effects between oxidation components and Fe-ZSM-5 in the SCR of NO by NH_3. However, there are a number of experimental details which seem incompatible with the simple model of a sequential mechanism of NO_2 formation and fast SCR providing this synergism. Closer inspection will, however, show that the model may indeed operate although a direct proof is difficult and different processes may also be involved.

It was found that mixtures of pure Mn oxides with Fe-ZSM-5 provided similar activities and selectivities as MnO_2-doped ceria zirconia oxide, which was studied by Stakheev et al. [10] as well. Further optimization would target suppression of the remaining N_2O selectivity and further increase of activity, probably achievable by using a more active Fe-ZSM-5 sample and by varying the ratio between catalyst components to get the optimum equimolar NO/NO_2 composition for fast SCR reaction.

Table 2
Crystal size of aged catalysts.

Catalysts	Crystal size (nm)
Aged Mn–Cu(2)	35
Aged Mn–Cu(2) + FeZSM5	30
Mn–Cr	41
Aged Mn–Cr + FeZSM5	46

Mn oxides are thermally very instable. Therefore, the rather mild thermal stress by the first SCR run caused drastic changes of the catalytic properties of oxidation components that were initially calcined at low temperatures: Mn(P) and the hopcalites (Figs. 2b and 4b). The total failure of the pure hopcalites is apparently due to the formation of large $(CuMn)_3O_4$ spinel particles (Fig. 1B). However, other pure oxidation components also suffered changes by the exposure to the feed at $T \leq 873$ K, e.g. Mn–Ce(CA) (compare Fig. 3a and b) although they had been previously calcined at an even higher temperature. It appears that redox processes possible in the feed can alter the surface in a different way than calcination in air.

In the mixtures with Fe-ZSM-5, solid-state reactions between oxidation component and zeolite might be an additional rationale for thermally induced changes of catalytic behavior between the first and second experiments. In particular, the behavior of Mn–Cu mixed oxides calls for an explanation involving solid-state reactions because the almost complete deactivation of the pure hopcalites by thermal stress (Fig. 4b) leaves little opportunity to explain a synergism via a gas-phase component: both NO and NH_3 passed the material almost unaffected up to 620 K. Solid-state reactions might include interactions between external zeolite surface and particles of the oxidation component leaving disorder of the latter in the affected region, or solid-state ion exchange (SSIE), which might interfere with phase formation during calcination in the presence of zeolite. SSIE could create intra-zeolite Mn and Cu sites. Mn zeolites do not offer any benefit to the SCR reaction in combination with Fe-ZSM-5 [21], but Cu zeolites are known to be highly active for standard SCR themselves [22,23] and to release N_2O as a by-product [24], which would comply with our observations. Therefore, XRD and XPS investigations were performed to shed more light on the actual origin of the behavior documented, in Figs. 3 and 4.

From the XRD patterns of Mn–Cu and Mn–Cr catalysts aged in 2% O_2/N_2 at 873 K for 1 h (Fig. 1B), it may be inferred that the zeolite component does not have significant influence on the formation of the $(CuMn)_3O_4$ spinel. Closer inspection showed that the spinel peaks are somewhat wider and less intense in the hybrid catalyst than in the absence of the zeolite, which is reflected in a larger crystal size determined for the latter case (Table 2). The zeolite seems to interfere with the growth of the crystals to some extent, but the effects are small. Therefore, it cannot be decided if this occurs by a specific interaction with the zeolite or just by the introduction of a diffusion resistance by the alien phase. In the case of Mn–Cr oxide, the intense signals of the $(CrMn)_3O_4$ spinel detected in pure Mn–Cr(CA) after its final calcination (Fig. 1A, trace c) were also found after joint calcination of this material with ZSM-5 (Fig. 1B, trace h). Here, the crystal size was slightly larger in the aged combined system (Table 2), which

may be explained by the longer exposure of this sample to high temperatures. Therefore, the XRD measurements did not provide evidence for significant changes to the oxidation component caused by interaction with the zeolite.

For copper, photoemission techniques provide a powerful tool to decide if Cu ions have entered the zeolite lattice. It is known that the Auger parameter (the sum of Cu 2p binding energy and Cu LMM kinetic energy) decreases strongly when Cu ions are dispersed within zeolites [25,26], which has been explained by the lower polarizability of the siliceous environment within the zeolite ([27], see also overview in [28]). Cu 2p and CuLMM spectra of Mn–Cu(2) have been measured after mixing with Fe-ZSM-5 and after calcination in 2% O_2/N_2 at 873 K for 1 h in the presence and in absence of Fe-ZSM-5. The spectra are shown in the supporting information (Fig. S1). In XPS, the satellite line of Cu 2p shows the copper clearly in the +2 state in the fresh Mn–Cu(2) while the signal splits into two after calcinations. One of them arises from Cu^{2+} again, while the other one appears at an unusually low binding energy and is difficult to assign. The signals measured in the presence and in the absence of zeolite are very similar. Therefore, this feature has not been further examined. Likewise, the Auger lines measured with Mn–Cu(2) calcined in the presence and in the absence of zeolite are similar. They are slightly shifted relatively to that of the fresh hopcalite, which should be expected given the formation of the $(CuMn)_3O_4$ spinel. There is, however, no indication for an Auger signal below 915 eV which would be indicative for intra-zeolite copper [25,26]. Hence, there was no solid-state ion exchange of Cu into the zeolite component of the hybrid catalyst during the aging treatment, where, however, the atmosphere differed from the reaction mixture by the absence of N-containing components.

Obviously, the activity and selectivity effects caused by aging are not easily explained on the basis of characterization data from classical techniques. Therefore, this problem will remain for future research. Actually, the proof for the mechanistic concept underlying the approach (consecutive mechanism NO_2 formation + fast SCR) does not seem to be straightforward either. There are definitely observations in favor of this concept: the high NO oxidation activities of pure MnO_2 and its synergy with Fe-ZSM-5, the only moderate attenuation of both effects by severe calcination of MnO_2, and the poor NO oxidation activity of Ce–Zr paralleling the lower SCR activity achievable with this component. The favorable influence of Fe-ZSM-5 on selectivity to N_2 (Figs. 2 and 6) is also compatible with the consecutive model. Thus, the onset of NO conversion over Mn(P) + Fe-ZSM-5 is almost identical with that over the pure Mn(P) (Fig. 2a), but the N_2O selectivity is significantly attenuated (Fig. 2c). Probably, the conversions measured result from both Mn and Fe sites, the former operating along their normal mechanism contributing some N_2O, the latter via fast SCR, which decreases the N_2O selectivity. Accordingly, Mn(CA) or Mn(P) in its second run contribute less own NO reduction conversion, which results in slightly decreased activity of the mixtures (Fig. 2a and b), but also significantly lower N_2O formation. Mn components with high own SCR activity like Mn–Ce(CA) are therefore unfavorable in terms of N_2O formation. When less active Mn compounds are used, the loss in activity might be outbalanced by employing a more active Fe catalyst.

The measurement of fast SCR conversions over pure Fe-ZSM-5 (Fig. 8) was meant to provide a limit for NO conversions expected from a mixed catalyst system that employs this reaction step, although the kinetics may be different between reaction regimes with presence of the equimolar NO/NO_2 ratio right from the start and with continuous formation of NO_2. Actually, the completely selective NO_x conversion of 60% achieved by Fe-ZSM-5 at 473 K was significantly exceeded only in two cases (Mn(P) + Fe-ZSM-5, Fig., 2a, Mn–Cu(1) + Fe-ZSM-5, Fig. 4a), which exhibited very significant formation of the side product N_2O under these conditions. Therefore, we cannot conclude a violation of this limit.

When, however, NO oxidation activities and synergistic effects are compared in more detail, contradictions are revealed. Mn–Cr(CA) is poor in NO oxidation (Fig. 7a), but forms a catalyst comparable with the other systems when combined with Fe-ZSM-5 (Fig. 3a). The NO_2 formation rates over Ce–Zr are lower than those of (fresh) Fe-ZSM-5 in a temperature range up to 670 K: they could not cause the synergy, which is clearly observed also below this temperature. Moreover, according to recent results, NO oxidation activities measured with fresh catalysts (i.e. the curve shown in Fig. 7a) are meaningless for discussions of mechanisms occurring in the SCR environment where NH_3 is present [20]. The contact with NH_3 (or with other reducing agents) causes so far non-identified changes in the structure of Fe species which can result in a drastic activation of the catalyst for NO activation (cf. Fig. 7c) [20].

With an NO oxidation activity as shown in Fig. 7c, it would be completely odd to expect synergistic effects between oxidation components as Mn–Cr(CA), Ce–Zr, Mn–Cu(1), Mn–Ce(CA) and this zeolite, which could better or equally well provide the NO_2 required by its own NO oxidation activity. But these effects clearly exist, and the problem is that NO oxidation to NO_2 over Fe-ZSM-5 is inhibited by NH_3 as described in literature [20,29]. Therefore, measurements of NO_2 formation rates in the absence of NH_3 are of no value for this mechanistic discussion. The crucial point is the extent of the inhibiting effect on NO_2 formation exerted by the NH_3 molecule, which has to be significantly smaller for the successful oxidation components than for Fe-ZSM-5, if the consecutive mechanism is to operate. Unfortunately, measurements of NO oxidation in the presence of NH_3 are difficult because adding ammonia to the NO/O_2 mixture will create the SCR feed, i.e., both reactions will interact. Indeed, the first indication of the inhibiting role of NH_3 on NO_2 formation came from a mathematical model of the reaction system over Fe-ZSM-5 [29], and our confirmation of this view has resulted from indirect reasoning [20]. Given these problems, we will confine ourselves to some qualitative statements for the case that the synergistic effect does proceed via the consecutive model (NO_2 formation + fast SCR) in the presence of NH_3. Under these conditions, the inhibition of NO_2 formation by NH_3 has to be very strong at the Fe sites in Fe-ZSM-5 as opposed to that at Ce sites on Ce–Zr (cf. Fig. 7c) because the NO_2 formation rate over Fe-ZSM-5 must be below that of Ce–Zr already at 573 K (Fig. 5a). The effect of NH_3 on the Mn sites must be very weak as well because the NO_2 formation rate over Mn–Cr(CA) must not fall short of that over Fe-ZSM-5 (Fig. 7).

As the present study aimed at outlining the synergistic effects to be achieved between oxidation components and Fe-ZSM-5, the data available so far only cover dry reactant mixtures. Any practical importance of these effects will, of course, depend on the response of the oxidation components, in particular, their NO oxidation activity, to poisons such as H_2O and SO_2. The impact of water on standard SCR over Mn-containing catalysts has been studied frequently and has been reported to be moderate or absent [7,8,10,30–32]. For SO_2, it is more severe even on a short timescale [7,8,31,32]. However, activities in standard SCR and NO oxidation are not necessarily correlated, as suggested by the different impact of thermal stress on activities in NH_3-SCR and in NO oxidation found with our MnO_x sample (Figs. 2a, b, 5a) and demonstrated by us recently for Fe-ZSM-5 [20]. Evidence on the influence of water on NO oxidation is scarce in literature, although conversion data for the reaction are sometimes reported—either in a dry or moist feed [8,10]. The fact that significant NO conversions could be achieved with Mn-containing catalysts in moist feed at a space velocity of 270,000 h^{-1} [10] lends the synergy concept some promise, and the synergy experiments with $Mn/Ce–ZrO_2$ described by Stakheev et al. were also performed

with water in the feed [10]. Research on poisoning influences on our synergetic systems, which will include SO_2 and durability testing is under way.

5. Conclusions

Combinations of Mn oxides and binary Mn–X (X = Ce, Cr, Cu) mixed oxides with Fe-ZSM-5 provide intense synergistic effects when used as catalysts for the selective reduction of NO with NH_3. Over wide temperature ranges, the NO conversions over these hybrid catalysts exceed the sum of conversions obtained with the individual components. In addition, the pronounced selectivity towards N_2O typical of Mn-containing systems is decreased in the presence of Fe-ZSM-5. While N_2O formation could not be completely suppressed in Mn-containing hybrids, by-products were nearly completely avoided with the combination of Ce–Zr oxide with Fe-ZSM-5, though at lower activity. The basic idea of these catalyst combinations, according to which an oxidation component converts some NO into NO_2 which enables Fe-ZSM-5 to react the remaining NO via fast SCR, could not be proved by measurements of NO oxidation activities. While these provided a general parallel trend between extent of synergy and NO oxidation activity, the NO oxidation activity of Fe-ZSM-5 in the absence of NH_3 exceeds or equals that of many oxides which provide significant synergistic effects. On the basis of recent results on the inhibition of NO_2 formation by NH_3 over Fe-ZSM-5, it has been concluded that the synergy may depend on a smaller inhibition of NO_2 formation over the successful oxidation components. Supporting data on NO_2 formation in the presence of NH_3 can be, however, made available only by kinetic modeling of the $NO/NH_3/O_2$ system because the SCR route is preferred over NO oxidation at such gas composition. Some of the hybrid catalysts exhibited remarkable changes after exposure to thermal stress, the origins of which have not yet been well understood.

Acknowledgements

We gratefully acknowledge experimental support by Dr. Thomas Reinecke (XRD), Ms. Noushin Arshadi (N_2 adsorption measurements), Dr. Ilya Sinev (photoemission) and Dr. Benjamin Johnson (photoemission, Fritz Haber Institute of Max-Planck Society, Berlin). We thank Dr. Stuart Tayler (Cardiff University) for providing hopcalite material from own development (cf. [17]). We also acknowledge donations of Carulite 300 by Carus Co. and of Ce–Zr mixed oxide by Umicore AG & Co. KG.

Appendix A. Supplementary data

Supplementary data associated with this article can be found, in the online version, at http://dx.doi.org/10.1016/j.apcatb.2014.10.018.

References

[1] J. Li, H. Chang, L. Ma, J. Hao, R.T. Yang, Catal. Today 175 (2011) 147–156.
[2] M. Kang, E.D. Park, J.M. Kim, J.E. Yie, Catal. Today 111 (2006) 236–241.
[3] M. Kang, E.D. Park, J.M. Kim, J.E. Yie, Appl. Catal. A: Gen. 327 (2007) 261–269.
[4] B. Thirupathi, P.G. Smirniotis, Appl. Catal. B: Environ. 110 (2011) 195–206.
[5] Z. Chen, Q. Yang, H. Li, X. Li, L. Wang, S. Chi Tsang, J. Catal. 276 (2010) 56–65.
[6] Z. Chen, F. Wang, H. Li, Q. Yang, L. Wang, X. Li, Ind. Eng. Chem. Res. 51 (2012) 202–212.
[7] M. Kang, T.H. Yeon, E.D. Park, J.E. Yie, J.M. Kim, Catal. Lett. 106 (2006) 77–80.
[8] G.S. Qi, R.T. Yang, R. Chang, Catal. Lett. 87 (2003) 67–71.
[9] G. Qi, R.T. Yang, R. Chang, Appl. Catal. B 51 (2004) 93.
[10] A.Y. Stakheev, G.N. Baeva, G.O. Bragina, N.S. Teleguina, A.L. Kustov, M. Grill, J.R. Thogersen, Top. Catal. 56 (2013) 427–433.
[11] G. Madia, M. Koebel, M. Elsener, A. Wokaun, Ind. Eng. Chem. Res. 41 (2002) 3512–3517.
[12] M. Schwidder, M. Santhosh Kumar, K.V. Klementiev, M.M. Pohl, A. Brückner, W. Grünert, J. Catal. 231 (2005) 314–330.
[13] M. Schwidder, S. Heikens, A. De Toni, S. Geisler, M. Berndt, A. Brückner, W. Grünert, J. Catal. 259 (2008) 96–103.
[14] G. Qi, R.T. Yang, Appl. Catal. B 44 (2003) 217–225.
[15] A. Trovarelli, Comments Inorg. Chem. 20 (1999) 263–284.
[16] B.M. Reddy, P. Lakshmanan, P. Bharali, P. Saikia, G. Thrimurthulu, M. Muhler, W. Grünert, J. Phys. Chem. C 111 (2007) 10478–10483.
[17] C. Jones, K.J. Cole, S.H. Taylor, M.J. Crudace, G.J. Hutchings, J. Mol. Catal. A 305 (2009) 121–124.
[18] M. Mauvezin, G. Delahay, F. Kißlich, B. Coq, S. Kieger, Catal. Lett. 62 (1999) 41–44.
[19] X. Zhang, Q. Shen, C. He, C. Ma, J. Cheng, L. Li, Z. Hao, ACS Catal. 2 (2012) 512–520.
[20] I. Ellmers, R.P. Vélez, U. Bentrup, A. Brückner, W. Grünert, J. Catal. 311 (2014) 199–211.
[21] L. Tillmann, M. Salazar, unpublished results.
[22] K. Rahkamaa-Tolonen, T. Maunula, M. Lomma, M. Huuhtanen, R. Keiski, Catal. Today 100 (2005) 217–222.
[23] T. Komatsu, M. Nunokawa, I.S. Moon, T. Takahara, S. Namba, T. Yashima, J. Catal. 148 (1994) 427–437.
[24] G. Delahay, B. Coq, S. Kieger, B. Neveu, Catal. Today 54 (1999) 431–438.
[25] B.A. Sexton, T.D. Smith, J.V. Sanders, J. Electron Spectrosc. Relat. Phenom. 35 (1985) 27–43.
[26] W. Grünert, N.W. Hayes, R.W. Joyner, E.S. Shpiro, M.R.H. Siddiqui, G.N. Baeva, J. Phys. Chem. 98 (1994) 10832–10846.
[27] J. Morales, J.P. Espinos, A. Caballero, A.R. Gonzalez-Elipe, J.A. Mejias, J. Phys. Chem. B 109 (2005) 7758–7765.
[28] W. Grünert, in: M. Che, J.C. Vedrine (Eds.), Characterisation of Solid Materials: From Structure to Surface Reactivity, Wiley-VCH, Weinheim, 2012, pp. 537–583.
[29] P.S. Metkar, N. Salazar, R. Muncrief, V. Balakotaiah, M.P. Harold, Appl. Catal. B 104 (2011) 110–126.
[30] P.R. Ettireddy, N. Ettireddy, S. Mamedov, P. Boolchand, P.G. Smirniotis, Appl. Catal. 76B (2007) 123–134.
[31] F. Liu, H. He, Catal. Today 153 (2010) 70–76.
[32] B. Thirupathi, P.G. Smirniotis, J. Catal 288 (2012) 74–83.